Mon. Not. R. Astron. Soc. **370,** 1612–1622 (2006) doi:10.1111/j.1365-2966.2006.10599.x

Cooling flows within galactic haloes: the kinematics and properties of infalling multiphase gas

Tobias Kaufmann,[1⋆] Lucio Mayer,[1] James Wadsley,[2] Joachim Stadel[1] and Ben Moore[1]
[1]*Institute for Theoretical Physics, University of Zürich, CH-8057 Zürich, Switzerland*
[2]*Department of Physics & Astronomy, McMaster University, 1280 Main St West, Hamilton, ON L8S 4M1 Canada*

Accepted 2006 May 18. Received 2006 May 17; in original form 2005 July 13

ABSTRACT

We study the formation of discs via the cooling flow of gas within galactic haloes using smoothed particle hydrodynamic simulations. These simulations resolve mass scales of a few thousand solar masses in the gas component for the first time. Thermal instabilities result in the formation of numerous warm clouds that are pressure confined by the hot ambient halo gas. The clouds fall slowly on to the disc through non-spherical accretion from material flowing preferentially down the angular momentum axis. The rotational velocity of the infalling cold gas decreases as a function of height above the disc, closely resembling that of the extra-planar gas recently observed around the spiral galaxy, NGC 891.

Key words: hydrodynamics – methods: *N*-body simulations – ISM: kinematics and dynamics – galaxies: formation.

1 INTRODUCTION

Galaxy formation is a complex process involving simultaneous action of many physical mechanisms. Even though we have a well-defined cosmological framework, Λ cold dark matter (ΛCDM), within which to study the galaxy formation, numerical simulations have achieved limited success as far as reproducing the structural properties of observed galaxies is concerned. Such simulations give rise to discs that are smaller and denser than their observed counterparts (e.g. Navarro & Benz 1991; Katz, Hernquist & Weinberg 1992; Navarro & Steinmetz 2000). A further problem is the difficulty in producing disc-dominated systems, even when haloes with quiet merger histories are selected. These problems may be due to the lack of a correct treatment of the physics of the multiphase interstellar medium, in particular of the balance between radiative cooling and heating from various forms of feedback arising from star formation (Navarro & Benz 1991; White & Frenk 1991; Katz et al. 1992; Robertson et al. 2004). However, limitations in the numerical models, for example the coarse mass and force resolution, are perhaps another major cause of the problem (Governato et al. 2004).

In this paper, we use new *N*-body+smoothed particle hydrodynamic (SPH) simulations, where we achieve a resolution in the gas component of 730 $M_{\odot}$, in order to follow the formation of a galactic disc via the cooling of gas within equilibrium dark matter haloes. Cosmological simulations suggest that the large discs of spiral galaxies form mainly from the smooth accretion of gas after the last major merger (Abadi et al. 2003; Sommer-Larsen, Götz & Portinari 2003; Governato et al. 2004). Therefore, although our simulations are not within the full cosmological framework, they are designed to follow the quiet gas accretion phase during the main epoch of disc formation. This allows us to resolve the cooling flow of gas at a very high resolution, which complements studies of disc formation within cosmological simulations.

The hierarchical formation of massive dark matter haloes, above a characteristic circular velocity of 120 km s^{-1}, is expected to efficiently shock heat the gas to their virial temperatures throughout the virial region (McCarthy et al. 2003; Dekel & Birnboim 2004). Angular momentum of the gas and dark matter is generated early by tidal torques, allowing it to cool and form a rotationally supported disc (Crampin & Hoyle 1964). The process of gas cooling from the halo into the disc is difficult to study observationally, and little evidence for gas accretion is observed in galaxies or cluster mass haloes. Cooling flow clusters are so named because of the observed decrease in the central temperature of the gas. In galactic haloes, the gas temperature can be lower than 10^6 K and thus difficult to observe by current X-ray telescopes (Benson et al. 2000), but there is evidence for a hot ionized corona surrounding the Milky Way.

Recent measurements of O VI and O VII absorption in the ultraviolet (UV) and X-ray part of the spectrum (Sembach et al. 2003) lend support to the idea that a lumpy gaseous Galactic halo exists and that such emission comes from the interface between warm clouds and the hotter diffuse medium. Maller & Bullock (2004, hereafter MB04) suggested that the gas supply to galaxies is mostly in the form of discrete warm clouds. Small density and temperature

⋆E-mail: tkaufmann@physik.unizh.ch (TK)

fluctuations are enhanced by the cooling process resulting in a runaway instability and the formation of a fragmented distribution of cooled material, in the form of warm ($\sim 10^4$ K) clouds, pressure-supported within the hot gaseous background. This model may explain the properties of high-velocity clouds (HVCs) around the Milky Way (Blitz et al. 1999), for example their radial velocity distribution and angular sizes.

Recently, Fraternali et al. (2005) measured the rotation curve of extra-planar neutral gas around the large spiral galaxy, NGC 891. This gas could be accreting material or gas falling back to the disc via a galactic fountain from star formation. The thermal instability mentioned above results in cloud masses that are predicted to be $\sim 10^6\,\mathrm{M}_\odot$, which is an order of magnitude below the minimum mass resolved in the SPH calculation in current state-of-the-art galaxy formation simulations (e.g. Governato et al. 2004). In this paper, we aim to have sufficient resolution to study the formation of a two-phase medium which will allow us to compare the kinematics of the gas with the observations of Fraternali et al.

The plan of this paper is as follows. In Section 2, we present the modelling of our haloes, the treatment of the cooling and the numerical techniques. In Section 3, we compare the kinematics of the gas and the disc with the observational data from Fraternali et al. The properties of the cool clouds are studied in Section 4, including survival times, mass function and numerical convergence studies. We conclude and summarize in Section 5.

2 INITIAL CONDITIONS AND METHODS

We set up a spherical equilibrium halo with a NFW profile (Navarro, Frenk & White 1996) and structural parameters consistent with predictions of the standard ΛCDM model (Kazantzidis, Magorrian & Moore 2004). We include a fraction of the total halo mass, f_b, as a hot baryonic component with the same radial distribution and a temperature profile such that the gas is initially in hydrostatic equilibrium for an adiabatic equation of state (EOS) for the gas. Of course, this kind of setup cannot model galaxy formation in general (no substructure, no counter rotation, etc), but should reproduce the late phase accretion after the last major merger. To illustrate the initial conditions, we plot the initial particle distribution and the density profiles in Fig. 1. The shape for the initial density of gas and dark matter is the same, whereas only the normalization is different. The curves after 0.5 Gyr show that the hot halo evolves out of equilibrium when using cooling, the density of the dark matter after 0.5 Gyr is enhanced in the centre due to adiabatic contraction.

The dark matter haloes are constructed using a multimass technique such that the innermost region is very well resolved. For the M33 'standard' model (see below), we use 1 400 000 particles distributed in the inner sphere of radius 20 kpc, then 600 000 particles in the next shell to 100 kpc, and the outer halo is resolved with 200 000 particles. This minimizes spurious heating of the gas particles due to collisions with dark matter particles (Steinmetz & White 1997) and enables us to resolve the dark matter cusp to ∼100 parsec. The reliability of these initial conditions is tested and reported in Zemp et al. (in preparation).

The gas has a specific angular momentum distribution and spin parameter consistent with values found for dark matter haloes within cosmological *N*-body simulations. The initial specific angular momentum profile is a power law following $j \propto r^{1.0}$, similar to the value $j(r) \propto r^{\alpha}$, $\alpha = 1.1 \pm 0.3$ found by Bullock et al. (2001). We also ran simulations with different angular momentum distributions to confirm that this does not affect the conclusions in this paper. The spin

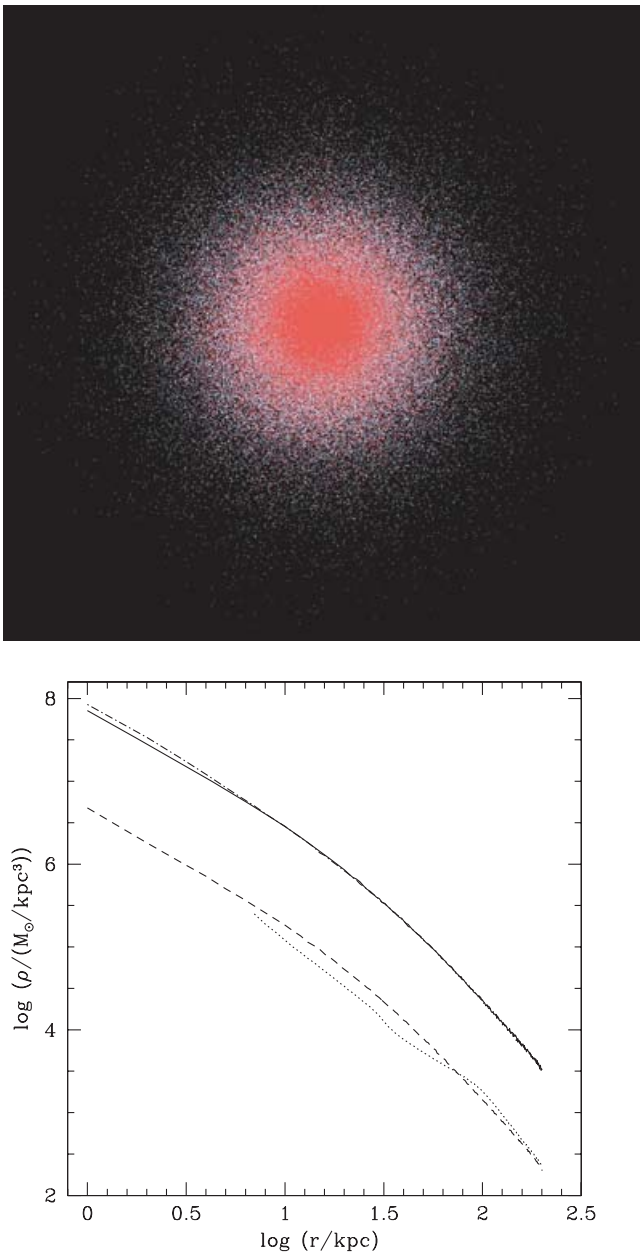

Figure 1. The upper panel shows the initial particle distribution (dark matter in white, gas in red; the box has a side length of 1200 kpc) and the lower panel the radial density profiles of gas and dark matter: the density of the dark matter initially is shown with a solid line whereas the dot–dashed line shows it after 0.5 Gyr. The dashed line shows the initial gas density and the dotted line the density of the hot gas outside the disc region.

parameter is $\lambda = \frac{j_{\mathrm{gas}}|E|^{0.5}}{GM^{1.5}}$, where j_{gas} is the average specific angular momentum of the gas, E is the total energy of the halo and G is the gravitational constant. This definition matches the one commonly used under the assumption that there is no angular momentum transport between the spherical dark matter halo and the gas. We carried out additional simulations where we set up angular momentum profiles by merging two equilibrium spherical haloes with different impact parameters. Both sets of simulations gave similar results. The detailed description of the runs is presented in Kaufmann et al. (2006).

We constructed dark plus gaseous halo models with parameters

Table 1. Simulation properties of the M33 models and cloud statistics for clouds identified with a FOF are shown. The minimum number of particles for objects to be identified with the FOF was set to be 32; in addition we also used 64 particles for the run with $N_{\rm SPH} = 64$, which gave the same result. The standard, refined_8 and refined_32 simulations are shown, respectively, in the fifth, sixth and seventh row. Rows eight and nine show two equal simulations differing only in the use of a minimal smoothing length. The final row shows the simulation with the enhanced cooling rate. The mass quoted in the second column is referring to the mass of one gas particle initially near the centre.

No. of dark/gas particles	m_g [$M_\odot$]	$T_{\rm cut-off}$ [Kelvin]	Time $(\rm Gyr)^{-1}$	$h_{\rm min}$	$N_{\rm SPH}$	Number of clouds	Total mass in clouds [$M_\odot$]
$2.5 \times 10^5/1 \times 10^5$	4.6×10^5	30000	1.5	–	32	0	0
$1.1 \times 10^6/5 \times 10^5$	9.2×10^4	30000	1.5	–	32	2	9.01×10^6
$2.2 \times 10^6/2 \times 10^6$	2.3×10^4	30000	1.5	–	32	13	1.23×10^7
$2.2 \times 10^6/2 \times 10^6$	2.3×10^4	30000	1.5	–	64	1	2.32×10^6
$2.2 \times 10^6/2 \times 10^6$	2.3×10^4	15000	1.5	–	32	13	1.52×10^7
$2.2 \times 10^6/3.9 \times 10^6$	2.9×10^3	15000	0.5	–	32	410	7.4×10^7
$2.2 \times 10^6/1.0 \times 10^7$	7.3×10^2	15000	0.5	–	32	3662	2.3×10^8
$2.2 \times 10^6/2 \times 10^6$	2.3×10^4	15000	0.65	–	32	7	8.46×10^6
$2.2 \times 10^6/2 \times 10^6$	2.3×10^4	15000	0.65	20 pc	32	11	1.03×10^7
$2.2 \times 10^6/2 \times 10^6$	2.3×10^4	30000	1	–	32	36	4.2×10^7

that are expected to produce discs similar to those of the Milky Way (MW model) and NGC 598 (M33 model). For the MW model, the virial velocity $v_{\rm vir} = 140$ km s^{-1}, virial radius $r_{\rm vir} = 200$ kpc, virial mass $M_{\rm vir} = 9.14 \times 10^{11}\,{\rm M}_\odot$, halo concentration $c = 8$, spin parameter $\lambda = 0.038$ and the baryonic fraction is $f_{\rm b} = 9$ per cent, and we resolve the gas halo with particles $\sim 2 \times 10^5\,{\rm M}_\odot$. For the M33 model, the parameters are $M_{\rm vir} = 5 \times 10^{11}\,{\rm M}_\odot$, $r_{\rm vir} = 167$ kpc, $v_{\rm vir} = 115$ km s^{-1}, $c = 6.2$, $f_{\rm b} = 6$ per cent and spin parameter $\lambda = 0.105$. In the standard M33 model, the hot gaseous halo is resolved with 2×10^6 particles of equal mass $\sim 2 \times 10^4\,{\rm M}_\odot$. To test further the effects of resolution, we performed simulations in which we use eight times as many SPH particles within the inner 30 kpc, the 'refined_8' M33 simulation. We split each SPH particle into eight 'child' particles (Bromm 2000; Kitsionas 2000; Escala et al. 2004). The new particles are randomly distributed according to the SPH smoothing kernel within a volume of size $\sim h_{\rm p}^3$, where $h_{\rm p}$ is the smoothing length of the parent particle. The velocities of the child particles are equal to those of their parent particle and so is their temperature, while each child particle is assigned a mass equal to $1/N_{\rm split}$, the mass of the parent particle. The new particles have a mass of $\sim 3000\,{\rm M}_\odot$. We then used the same method to create the 'refined_32' M33 simulation, where each SPH particle within the inner 30 kpc has been split into 32 particles having masses of $\sim 730\,{\rm M}_\odot$. An overview to the M33 simulations can be found in Table 1.

We use the high-performance parallel Tree+SPH code GASOLINE (Wadsley, Stadel & Quinn 2004), which is an extension of the pure N-body gravity code PKDGRAV developed by Stadel (2001). It uses an artificial viscosity which is the shear reduced version (Balsara 1995) of the standard Monaghan (1992) artificial viscosity. GASOLINE uses a spline kernel with compact support for the softening of the gravitational and SPH quantities. The energy equation is solved using the asymmetric formulation

$$\frac{{\rm d}u_i}{{\rm d}t} = \frac{P_i}{\rho_i^2} \sum_{j=1}^{n} m_j \boldsymbol{v}_{ij} \cdot \nabla_i W_{ij}, \qquad (1)$$

where u_i, P_i, ρ_i, m_i, $\boldsymbol{v}_{ij}$ and W_{ij} are the internal energy, pressure, density, mass, velocity and a kernel function, respectively. This formulation is shown to yield very similar results compared to the entropy conserving formulation but conserves energy better (Wadsley et al. 2004). In a test problem with an expanding sphere and no gravity, the entropy conservation for each particle as measured by the temperature error has a rms error of 3 per cent for a factor of 10 change in density; however, this is a very conservative estimate since in situations of astrophysical interest entropy conservation should be measured against the other contributors to changes in entropy, namely shocks and cooling, and these are expected to be dominant, especially in the case of a gravitational collapse. In all the runs, we included Compton and radiative cooling using a standard cooling function for a fully ionized, primordial gas of helium and hydrogen. The radiative losses per step are limited to no more than 25 per cent per dynamical step, and the cooling can adapt the time-steps to suit its needs. The density changes are quite slow – occurring on the dynamical time-scale and typically less than 1–2 per cent per step. Therefore, the assumption of a constant density in one time-step contributes only a small error to the cooling rates, especially compared to missing coolants such as metals. Because of the lack of molecular cooling and metals, the efficiency of our cooling function drops sharply below 10 000 K. Moreover, we used an artificial lower limit for the gas temperature (15 000 or 30 000 K), higher than the cut-off in the cooling function, to crudely model the effect of the UV background and stellar feedback (see e.g. Barnes 2002). This temperature floor is also required to avoid the onset of a violent gravitational instability and fragmentation of the gaseous layer after the disc begins to assemble.

For the identification of the clouds, we use a friends-of-friends algorithm (FOF), using 32 particles (equal to the number of particles in the smoothing kernel) as the threshold. The linking length was chosen to be of the order of 0.3 the mean particle separation in the standard run; it was then lowered for higher resolution (according to the smaller mean particle separation), and we checked in the standard simulation that the number of clouds found with the FOF does depend only weakly on the exact choice of the linking length.

3 THE ASSEMBLY OF THE DISC

Due to cooling, the hot gas halo loses its hydrostatic equilibrium configuration quite quickly (see Fig. 5). The inner disc rapidly forms from cooling gas from a nearly spherical region close to the centre (within $\sim$10 kpc) of the halo. The accretion rate of cold gas slows down with time, and the outer disc region forms from material which flows preferentially down the angular momentum axis. This leaves a 'cylindrical' region of hotter and less dense gas above and below the disc plane as is evident in Fig. 2. This non-spherical inflow of gas

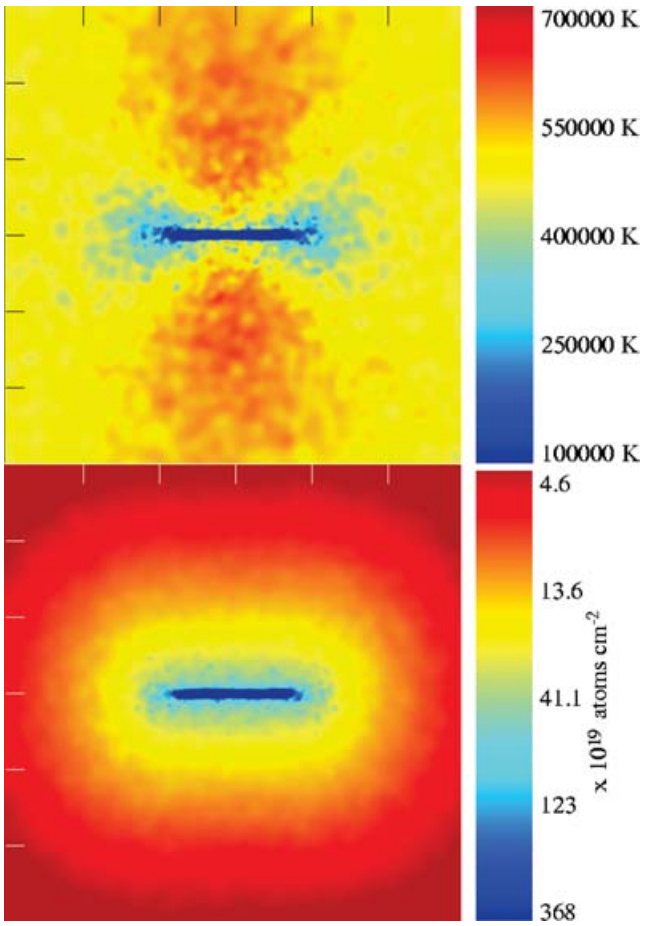

Figure 2. The two panels show colour maps of projected temperature (upper map) and density (lower panel) after 2.1 Gyr of the standard M33 model (see text). The box has a side length of 60 kpc. The hotter and less dense gas above and below the disc is visible (see text for details).

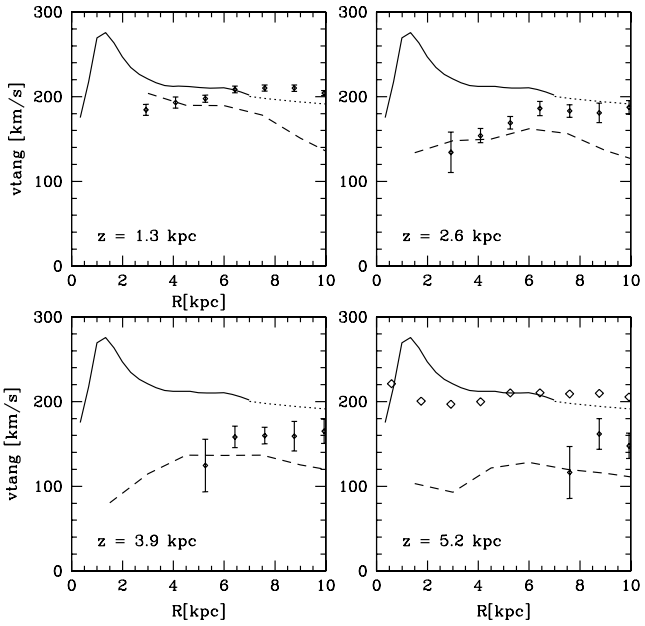

Figure 3. The solid lines show the physical rotational velocity of the gas in the disc plane of the MW model. The dashed lines in the different panels show the rotational speed at various distances above the galactic plane. The vertical velocity gradients in the model are 16, 21, 19 and 17 km s^{-1} kpc^{-1}, respectively. The open symbols in the last panel show the observed rotational speed of NGC 891 in the disc plane, and the points with error bars in the panels show the observations above the plane of the galaxy. The rotation curve in the disc of NGC 891 is scaled such that the flat part matches the rotation curve in the disc plane of our simulation; the rest of the data and also height z above the disc are then scaled with the same factor.

from the halo to the disc is not currently considered in semi-analytic models for disc formation.

As expected, the higher angular momentum M33 model produces a more extended disc than the MW model. Furthermore, the morphology of the discs within the two models is very different. The higher baryon fraction and lower spin parameter of the MW model give rise to a disc that dominates the mass distribution in the inner region. The MW model forms a bar in the very early stages and has the appearance of an Sb galaxy, whereas the M33 model resembles a galaxy of type Sc–Sd, with a smoother, more flocculent spiral pattern. Even though the M33 model does not undergo bar formation, the cooling gas forms a dense central nucleus which has a size of the order of our length resolution of a few hundred parsec. The global morphological evolution of both models depends on the mass and force resolution and is discussed in Kaufmann et al. (2006). Here, we present the analysis of the kinematics of the cooling gas.

3.1 Gas infall and extra-planar gas

Fraternali et al. (2005) observed the rotation velocity of neutral gas as a function of scaleheight above the disc for the galaxy, NGC 891, which has a luminosity and rotational speed similar to the Milky Way. They found extra-planar neutral gas up to distances of 15 kpc above the plane and a velocity gradient of about -15 km s^{-1} kpc^{-1} in the vertical direction. The gas closest to the disc, at $z < 1.3$ kpc, appears to corotate with it, but they argue that due to the limited angular resolution this may be the effect of beam-smearing. They considered a galactic fountain model in order to explain these observations, but that model failed to reproduce the amount of lagging. They argue that gas accretion may be important as well in these situations.

Here, we present results from our MW simulation where we show that this velocity gradient arises naturally in the accretion phase of the gas as it falls on to the galactic disc. Fig. 3 shows the rotational velocity of the gas as a function of height above the disc in our MW simulation. We plot the actual circular rotational speed of the gas averaged over the annulus at the given radii. (Note that this is slightly different from the observations which measure the projected rotational speed at a given radius.) The central velocity curve has a bump due to the bar formation and the excess of low angular momentum gas in the inner halo. The decrease in rotational velocity above the plane matches the observations quite well. This suggests that the observations of Fraternali et al. (2005) support the idea that discs form via the cooling flow of gas which is rotating faster closer to the disc by conservation of angular momentum.

In Fig. 3, we plot the rotational speed of all the gas as a function of position above the disc plane, and not just gas in the neutral phase such as measured by Fraternali et al. (2005) However, in a recent observation of NGC 891 by Heald et al. (2005), it has been found that the velocity gradients of the hot gas agree with the results for the neutral gas. As we then increase the resolution, we find that the hot

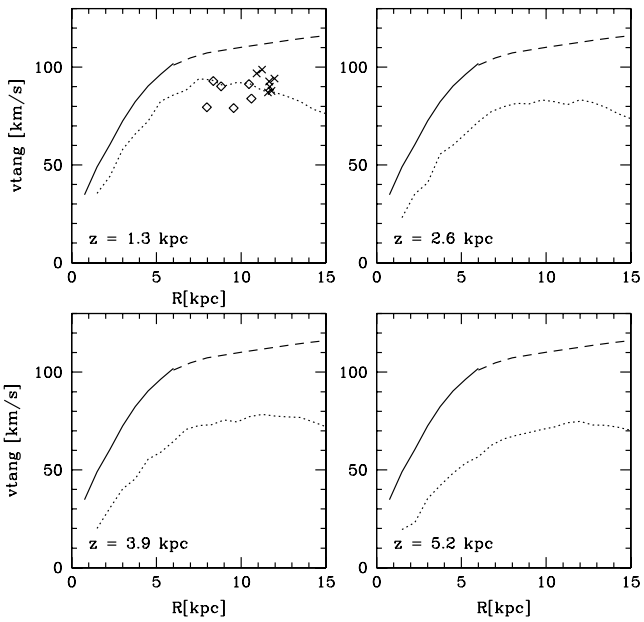

Figure 4. The solid lines show the physical rotational velocity of the gas in the disc plane of the M33 model after 2 Gyr (dashed lines show circular velocities). The dotted lines in the different panels show the rotational speed at various distances above the galactic plane of all the gas in the respective plane. The open symbols show the tangential velocities of the cold clouds near the disc, which are between $z = 1.3$ and 2.4 kpc away from the galactic plane, and the crosses mark clouds which are at distances of less than 1.3 kpc. The calculated velocity gradients (from all the gas) are 8, 8, 6 and 6 km s^{-1} kpc^{-1}, respectively, whereas we get 6 km s^{-1} kpc^{-1} for the velocity gradient derived from the clouds.

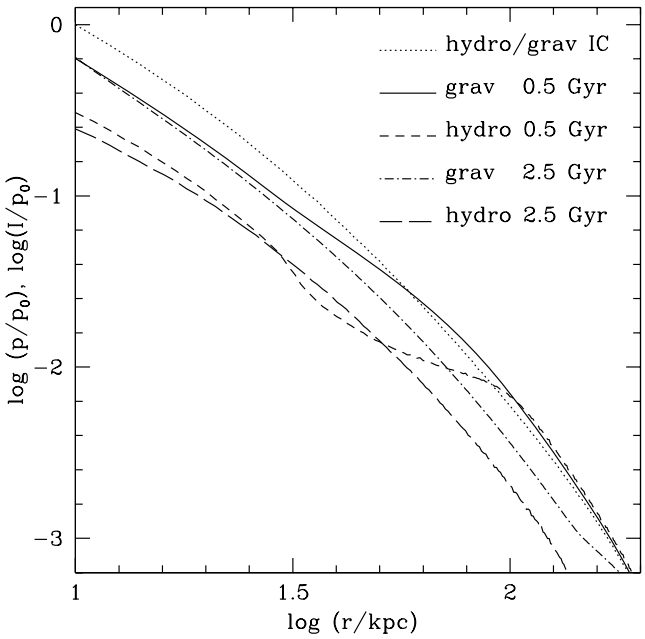

Figure 5. The time-evolution of the pressure in the hot gas halo and the gravitational attraction [$I \equiv \int_R^\infty G\rho_g(r)\frac{GM(r)}{r^2}\,\mathrm{d}r$] is plotted versus radius (standard M33 run). Initially, gravity and pressure were balancing each other, at later times the gas halo has lost pressure support due to cooling.

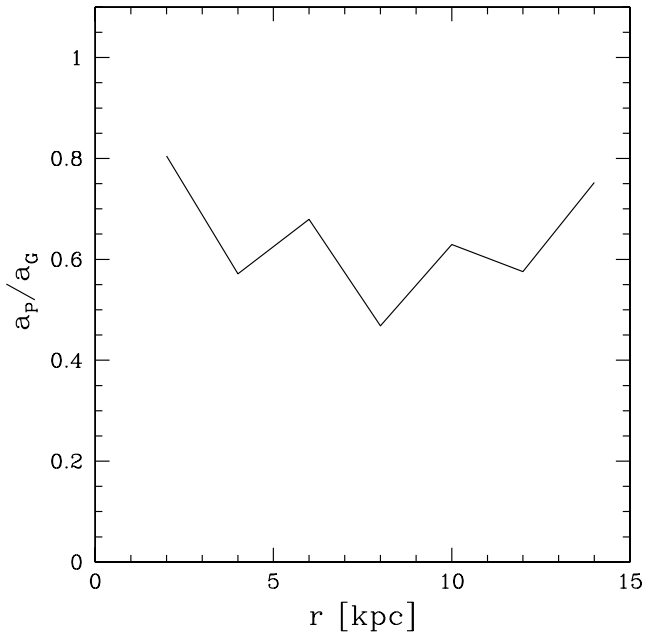

Figure 6. The ratio between hydrodynamical and gravitational acceleration in the z-direction (perpendicular to the disc) is plotted versus radius. For this measurement, gas particles in a box were chosen, the box is 2 kpc above the disc centre and has a height of 1 kpc; the model is 2 Gyr old. In average, the hydrodynamical acceleration is ≈60 per cent of the gravitational acceleration.

halo is thermally unstable and forms dense gas clouds which then accrete on to the disc. These clouds may cool down and become partially neutral (see Section 4.2). We only achieve the resolution necessary to observe this two-phase medium in our M33 model (see Fig. 4 for the corresponding velocity plot), but such clouds would occur also in the MW model if we had sufficient resolution. Unfortunately, due to the higher baryonic density in the centre of the MW model this simulation is much more demanding computationally since particles require shorter time-steps. The cool clouds in the M33 rotate at a comparable speed as all the gas, which justifies the measurement of the kinematics within all the gas. The determination of the velocity gradient from the cold clouds alone was only possible in the inner region, because there were too few clouds at higher z in the standard M33 model, but we get a comparable number as if we take all the gas in the plane (Fig. 4). Fig. 5 shows that the hot gas halo cannot preserve pressure support for an EOS with cooling. The infall of the hot gas is therefore expected.

The hydrodynamical forces due to diffuse hot corona on the infalling gas are substantial: the infall velocity in the M33 galaxy of the gas above the disc is approximately 10 km s^{-1}. This is much smaller than the pure free-fall velocity towards the disc, ∼70 km s^{-1}. This radial infall velocity agrees well with that observed by Fraternali et al. (2002) of approximately 15 km s^{-1} for NGC 2403, a galaxy similar to M33. In Fig. 6, we show the ratio between pressure (hydrodynamical) and gravitational accelerations perpendicular to the disc for some gas particles 2 kpc above the disc. The pressure forces can equilibrate the gravitational forces in average at the ≈60 per cent level, which results in this lowered infall velocity. The result for particles which are, for example, 20 kpc above the disc is similar.

4 DISC FORMATION VIA ACCRETION OF A CLUMPY MEDIUM

MB04 proposed that discs form via the accretion of warm clouds that develop from thermal instabilities in the hot gaseous halo (see also Mo & Miralda-Escude 1996). This instability arises as small density

fluctuations cool faster than most of the surrounding gas; cooling amplifies these density fluctuations further and the instability grows rapidly. According to MB04, this clumpy formation of disc galaxies would at the same time explain the existence of HVCs and give rise to a characteristic upper limit on the masses of galaxies consistent with observations. Typical parameters for the clouds in a Milky Way sized halo today would be a size of ∼1 kpc and a characteristic cloud mass of $\sim 5 \times 10^6\,\mathrm{M}_\odot$. Several physical mechanisms, for example the Kelvin–Helmholtz instability and conduction, impose a lower mass limit on clouds that can survive (see below). These clouds have not been found in cosmological simulations of galaxy formation since even the highest resolution studies have a single SPH particle mass equal to the expected characteristic cloud mass (Sommer-Larsen et al. 2003; Governato et al. 2004).

4.1 Formation of pressure-confined clouds

In the M33 model, we can achieve a higher resolution since the lower density cold component requires less computational work. In the standard M33 model, the force resolution is 100 pc or ∼0.06 per cent of the virial radius, and the SPH particle mass is $2 \times 10^4\,\mathrm{M}_\odot$. These simulations produce a large population of warm ($T \sim 10^4$–10^5 K), high-density, pressure-confined clouds that are forming within the hot ($T \sim 10^6$ K), gaseous halo (see Figs 7 and 8). These clouds eventually cool down to the temperature floor in our cooling function and would contain substantial fractions of neutral hydrogen. We will discuss the behaviour below the temperature floor in Section 4.2.3. These clouds are in pressure equilibrium with the halo gas – their gravitational binding energy is typically 50 times smaller than the thermal energy, hence the clouds are not gravitationally bound. The clouds have radii of 0.1–0.6 kpc and masses from 10^5 to a few $10^6\,\mathrm{M}_\odot$. As expected, a lower number of clouds is found for a higher number of particles in the SPH smoothing kernel, but at the standard resolution we still see a cloud smoothing over 64 neighbours (Table 1). The parameters of the different simulations and the properties of the clouds are shown in Table 1.

The thermal instability starts because of small density fluctuations present in the initial SPH particle distribution. These fluctuations grow rapidly, increasing in size and density until a pressure-confined cold cloud forms. In reality, these fluctuations might be driven by external perturbations, for example infall of cold gas and substructure or turbulence induced by supernova winds from disc stars or a galactic fountain. The temperature fluctuations are clearly visible throughout the gaseous halo in the left-hand plot of Fig. 9. These cold pressure-confined clouds are seen only within about 10 to 20 kpc from the disc. This may be a SPH resolution effect – further out in the halo the gas density is lower and the SPH smoothing length is much larger. Thus, density and temperature fluctuations are suppressed by the smoothing.

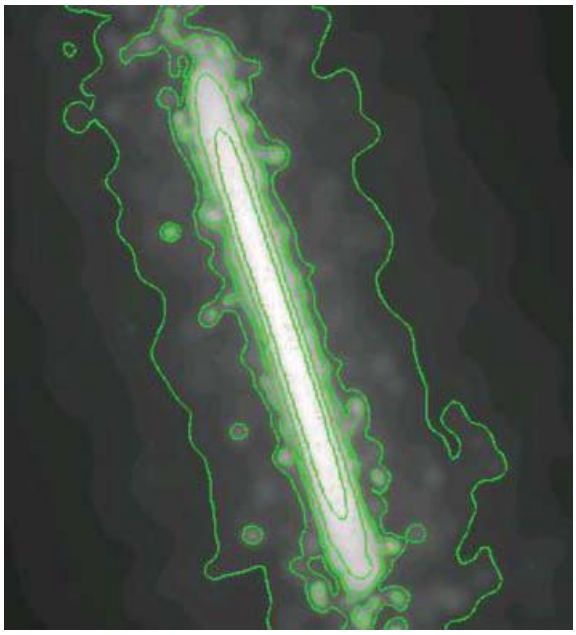

Figure 7. The projected gas density of the standard M33 model after 1.5 Gyr shows a clumpy/irregular outer contours similar to that observed in NGC 891. The outer contour shows a gas surface density of $\sim 10^{20}$ atoms cm^{-3}.

One of the conditions for cloud formation is that the sound-crossing time, $\tau_\lambda \simeq \lambda_i / v_s$, across a perturbation of wavelength λ_i, should be less than the characteristic cooling time (MB04). If this condition is not satisfied, the perturbation is erased because the local cooling time is too close to the mean cooling time and the whole region becomes isothermal. In our simulations, we can resolve perturbations in the gas to $\sim 2h$, where h is the smoothing length in the SPH code. We tested this condition in regions around the disc (20 kpc from the centre) where no clouds formed and found that $\tau_\lambda > \tau_{\mathrm{cool}} = \frac{E}{|\dot{E}|} = \frac{T}{|\dot{T}|}$ (here we took $\lambda_i \sim 2h$) even at quite low temperatures ($T \approx 30\,000$ K). For regions where clouds form, the condition $\tau_\lambda < \tau_{\mathrm{cool}}$ is fulfilled where the values of the smoothing length $h \approx 0.65$ kpc.

In order to assess the growth rates and resolution dependence of the instability, we performed simple tests using SPH particles distributed randomly in a 10-kpc periodic cube with initial temperature

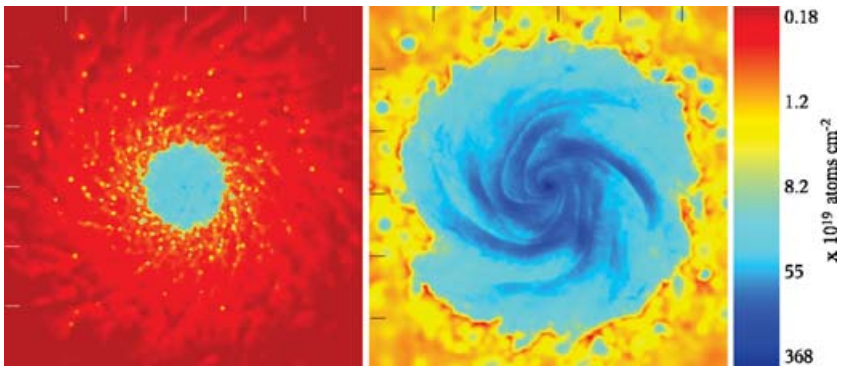

Figure 8. Density maps of gas in a slice through the centre of the M33 gas disc in boxes of length 40 kpc (left-hand panel: refined_8 resolution simulation after 0.5 Gyr) and 20 kpc (right-hand panel: standard resolution after 2.1 Gyr). The high-order spiral pattern closely resembles that of Sc/Sd galaxies.

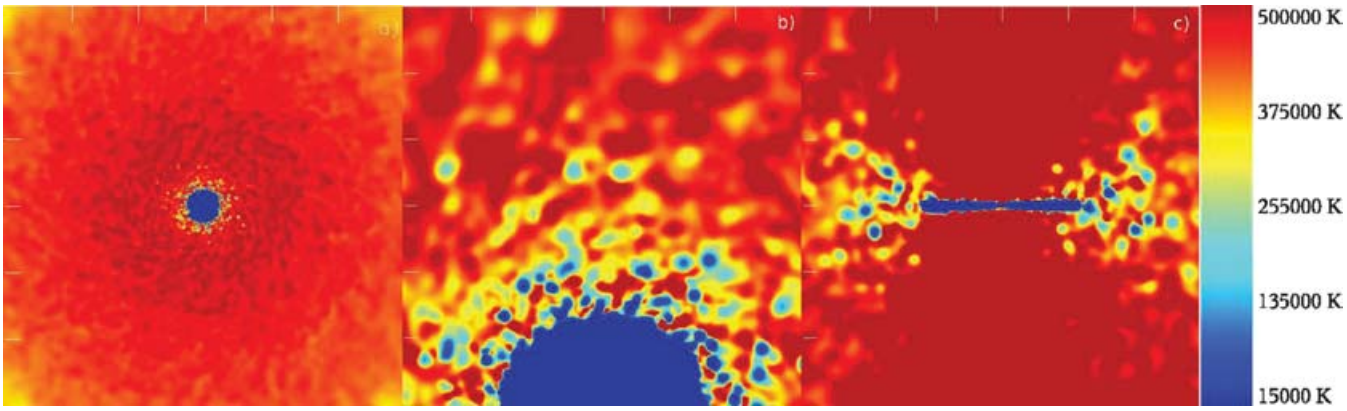

Figure 9. Temperature maps of the gas in slices through the centre of the standard M33 simulation after 2.1 Gyr. Panels (a) and (b) show 200 and 32 kpc regions, respectively. Panel (c) shows a 40-kpc slice perpendicular to the disc plane.

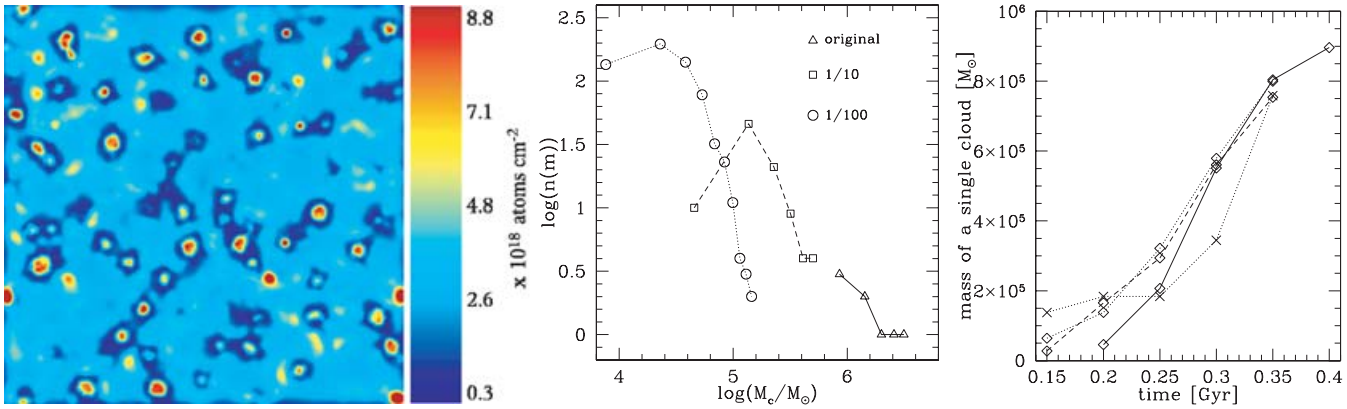

Figure 10. The left-hand panel shows a colour density map of a slice through the centre of the highest resolution cube simulation after 0.4 Gyr, where red indicates denser regions. The central panel shows the mass distribution of the clouds after 0.4 Gyr. The right-hand panel shows the mass growth rate of a single cloud: the cube simulations are plotted with open symbols where the solid lines show the original resolution, dashed line intermediate scaled by a factor of 4 and dotted line is the highest resolution scaled by a factor of 40. A cloud from the standard M33 simulation is marked with crosses. In the latter case, growth via merging begins after 0.25 Gyr.

($T = 450\,000$ K) and density ($n_{\rm H} = 0.01$ cm^{-3}) comparable to those from the central region of the halo models. We ran three simulations with particle masses 1, 1/10th and 1/100th times those in the full halo simulations. We found cold gas clouds forming above the 32 particle SPH smoothing kernel which grow linearly with time and mass (see Fig. 10). The higher resolution simulations produce the smallest clouds since they have lower average Poisson fluctuations. After 0.8 Gyr, the whole box thermalizes as the medium surrounding the clouds has had time to cool down to roughly the same temperature of the clouds. At this point, the clouds dissolve into the outer medium since they are not pressure confined any more and the instability saturates.

We can compare the growth rates to those in Burkert & Lin (2000), which derived a condition for exponential versus linear growth in a static, thermally unstable gas layer: the ratio of the initial cooling to sound-crossing time-scale K_j has to be larger than the critical value $K_{\rm crit}$, where

$$K_j = \tau_{\rm cool}(0) k_j \sqrt{R_g T_0(0)/\mu}, \tag{2}$$

$$K_{\rm crit} = \left(\frac{\rho_{\rm a}}{\rho_0}\right)^{(2\beta-3)\Gamma/(4-2\beta)} \tag{3}$$

and where $\tau_{\rm cool}(0)$, k_j, R_g, μ, $T_0(0)$, Γ and β are the characteristic cooling time-scale at time 0, wavenumber, gas constant, initial temperature, mean molecular weight, adiabatic index and the exponent of the power law of the cooling rate, respectively. $\rho_{\rm a}$ is the initial perturbation amplitude and ρ_0 the initial mean density. The paper by Katz, Weinberg & Hernquist (1996) shows the cooling rate of a primordial composition gas (as is used in GASOLINE), for $3 \times 10^4 < T < 10^6$ a power law with $\beta = -1$ gives a rough approximation; with $\Gamma = 5/3$ we find $K_{\rm crit} \approx 24.5$ for simulation with the 10 per cent overdensity. For K_j, we get ≈46.8 using $\tau_{\rm cool}(0) = 0.04$ Gyr, $T_0(0) = 450\,000$ K and taking two times the mean smoothing length as the smallest wavelength which is resolved ($\lambda_{\rm min} = 0.16$). Therefore, the calculated K_j is not a mean K_j but the maximal one, its value is roughly two times bigger than the critical value; however the mass (and density) growth remains linear over several cooling times (Fig. 11). An additional reason for this may be because at around 10^5 K the real cooling curve decreases over several tens of thousands of Kelvin and would therefore damp an instability.

The thermal instability generated in the cubes is purely of numerical origin since it is seeded by the initial Poisson fluctuations. A higher resolution setup simply starts with lower amplitude of the initial fluctuations, hence the different mass of the transient clouds formed. The following step is thus to impose a perturbation and study

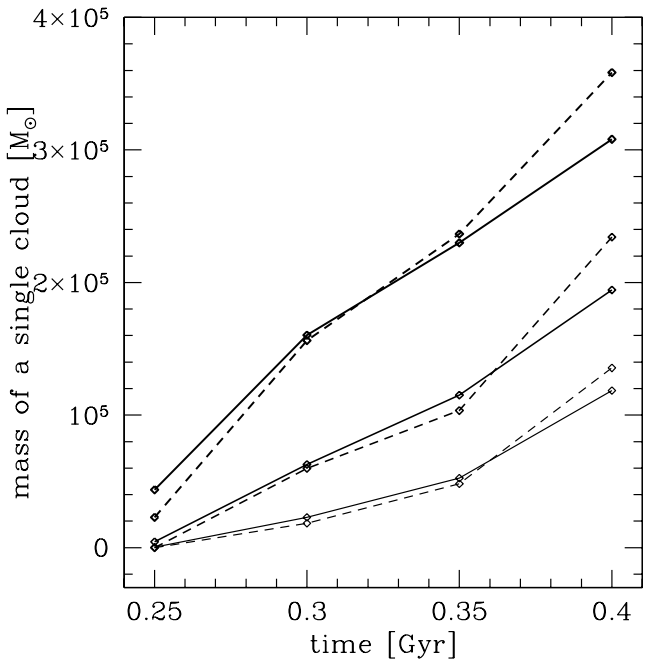

Figure 11. The mass-growth rate of a single cloud in the box simulation with spherical overdensity is shown. The highest and intermediate resolution are plotted with solid and dashed lines, respectively. The thicker the lines the bigger was the initial overdensity (10, 20 and 40 per cent). The mass growth was close to linear, and the results for the different resolutions nearly converge.

how the system responds when we increase the resolution. This way, we can assess robustly the dependence on resolution since the initial perturbation is independent of resolution. We used the cubes with particle masses 1/10th and 1/100th times those in the full halo simulations. To wash out initial Poisson noise, the cubes were evolved for 5 Gyr using an isothermal EOS (with the same temperatures and mean density as before). Then, we placed a spherical overdensity at an arbitrary location within the box. We run three different models where the overdensity was on the 10, 20 and 40 per cent level, respectively, at both resolutions. We find that the mass of the clouds in this case, just before the whole box thermalizes, differs roughly by the same factor as the initial overdensity, the growth rate is linear in time as in the previous cube tests and the results in the two resolutions nearly converge (see Fig. 11). In passing, we note that the results at 0.4 Gyr probably overestimate slightly the cooled mass due to the overdensity, because in the next time-step the whole box has already thermalized. The fact that we found nearly convergent results has important implications for the collapse simulations that we discuss below. In fact, the intermediate resolution test has particle masses comparable to the 'refined_8' M33 simulation, which should thus have enough resolution to properly resolve the thermal instability for an initial amplitude of the fluctuations 10 per cent or higher.

So far, we had built-in or imposed perturbations as seeds for the thermal instability. We can ask if there is a reasonable way of producing perturbations of the order of 10 per cent or larger, namely of the same magnitude of those existing in the initial conditions of the full simulations. One way these perturbations can be produced is by dark matter and baryonic substructure in galactic haloes. We carried out an additional test run using the high resolution periodic cube. We added a massive particle with characteristic size (i.e. gravitational softening) and mass comparable to the Magellanic Clouds. The particle moves through the box at a speed of $\sim$200 km s^{-1} as expected for a dwarf galaxy satellite orbiting in the Milky Way halo. Starting with an isothermal EOS, we saw that the particle rapidly triggered the formation of a trailing overdensity well above 20 per cent of the background density just behind. Evolved with cooling, this overdensity grew considerably faster than the fluctuations due to numerical noise, as expected from its larger amplitude. Clearly, we have chosen a favourable case, since most of the galactic satellites are lighter than the Large Magellanic Cloud (LMC) and would drive weaker perturbations. Triggering of gas density fluctuations by substructure in a CDM halo should indeed be dominated by the many dark satellites at least 100 times lighter than the LMC. Individually, these would drive perturbations that are too small to grow significantly on a dynamical time. However, perturbations presumably would not be isolated but would interact, possibly amplifying more rapidly than expected from the linear growth. This is already suggested by the fact that clouds in the full simulations grow faster than in the cube tests due to merging. The presence of a clumpy medium near the disc, which we invoked to explain the observations of Fraternali et al. in previous sections, would suggest that there must be a source of the perturbations acting near the disc, fairly isotropic and active even at the present epoch. Whilst satellite accretion of fly byes may have been frequent enough early in the galaxy formation process to be a major source of perturbations near the disc, other mechanisms are probably responsible for triggering the thermal instability today. Galactic fountains driving turbulence in the inner part of the hot gaseous corona might be one possibility. We will address the question on the physical origin of those perturbations in an upcoming paper.

There are important differences between all the cube tests performed and the full simulation. One that we just mentioned is that in the full simulations clouds can grow faster due to mergers with other nearby clouds (see Fig. 10). Another one is that the perturbations are not growing out of a static gaseous background as in the cubes but within infalling hot gas. The static case was recently investigated in Baek et al. (2005) where a perturbation at the 20 per cent level was used to produce clouds with masses of about 10^5 M$_\odot$ using a grid code. In a similar spirit, Fall & Rees (1985) showed that an initial density perturbation of the order of 10 per cent of the average density is needed to produce clouds with masses comparable to those of globular clusters in an infalling medium. This is consistent with the fact that in the full simulations the initial perturbations are larger than 10 per cent, so that one expects the thermal instability to be able to produce fairly massive clouds.

In order to test the effects of resolution directly in the full simulations, we have run two simulations with particle splitting. First, we carried out the refined_8 M33 simulation. Particles within the refined sphere of 30 kpc reach the disc in about 1.5 Gyr. By running the simulation only up to 1 Gyr, we make sure that there is no contamination of heavier particles in the disc, which can lead to spurious results (Kitsionas 2000). The splitting scheme should preserve the amplitude of perturbations at large scales that were present in the original simulation, while noise at previously unresolved scales should trigger the formation of smaller clouds. After 0.5 Gyr (see Fig. 8 and Table 1), there are about 700 resolved clouds with mean mass 1.8×10^5 M$_\odot$, up to 19 kpc from the centre. The most massive cloud has a mass of 1.1×10^6 M$_\odot$, which is comparable to the most massive cloud (1.6×10^6 M$_\odot$) in the standard M33 simulation *at the same time*. We then performed an even higher resolution run by splitting the initial particle distribution by an additional factor of 4. In the refined_32, there were more than 4300 clouds having more than 32

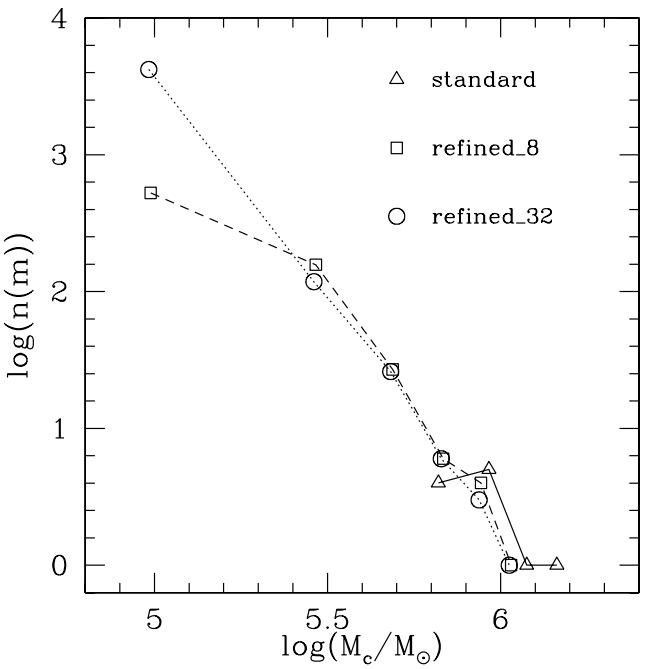

Figure 12. The mass distribution of clouds in the M33 simulation after 0.5 Gyr, where the dotted, dashed and solid curves show the refined_32, the refined_8 and standard resolution simulations (see text and Table 1), respectively.

particles due to the smaller perturbations. The large-scale perturbations were followed similarly in all these three simulations, resulting in a comparable mass distribution of the clouds at the high-mass tail (see Fig. 12). The satisfactory convergence at the scales resolved by all simulations is not a trivial result; it shows that the amplification of the perturbations is numerically robust even in complex simulations such as those in which the gas density does not only change simply because the local cooling rate changes but also changes as a result of compressions and shocks driven by the gravitational collapse. In other words, only the initial amplitude of the fluctuations is not self-consistently determined.

4.2 Evolution and dissolution of the clouds

In the standard M33 run, a typical compact cloud has a mass of $\sim 1.1 \times 10^6\,\mathrm{M}_\odot$ and a temperature equal to the cut-off temperature in the cooling function ($T_{\rm cloud} = 15\,000$ K), radius $R \sim 0.2$ kpc and lifetime of $\sim$0.1 Gyr (from formation to entering the disc). We now investigate the mechanisms that could disrupt or modify the structure of cold clouds embedded in a hot medium.

4.2.1 Kelvin–Helmholtz Instability

As a cool, dense cloud moves through a hot, tenuous background, the interface between the two phases is subject to the growth of Kelvin–Helmholtz instabilities. At our resolution, SPH does not resolve such instabilities due to smoothing and the artificial viscosity which tends to blur any sharp interface between the inner and outer medium. In other words, the Reynolds number is always lower than the Reynolds number expected in turbulent flows where the Kelvin–Helmholtz instability can develop (see Mayer et al. 2006). For the case in which gravity is unimportant, Murray et al. (1993) derive a characteristic growth time for the instability of

$$\tau_g \approx \frac{R_{\rm cloud}(\rho_{\rm cloud}/\rho_{\rm bg})^{0.5}}{U}, \tag{4}$$

where U is the relative velocity and $\rho_{\rm bg}$ is the density of the background medium. The clouds are therefore expected to break up on time-scales comparable to τ_g. In their numerical experiments, they actually found that the mass loss was still quite small over time-scales twice as long as τ_g. In our simulations, the density contrast is $\approx$100, the relative velocity U is $\approx$10 km s^{-1}, and therefore we end up with $\tau_g \approx 0.2$ Gyr using 0.2 kpc for the radius of the cloud. Since such time-scale is longer than the typical lifetime of the clouds, we expect the effect of the Kelvin–Helmholtz instability to be negligible.

The radial infall velocities are of the order of 10 km s^{-1}, which is insufficient to perturb the cloud structure. As the halo gas density becomes lower, we might expect clouds to infall faster. Observations of the radial motion of clouds could therefore be used to constrain the ambient halo density.

4.2.2 Conduction

In principle, conduction can prevent the growth of small clouds. MB04 suggest random magnetic fields reduce conduction by at least an order of magnitude (the reduction could be much stronger if the field is uniform or tangled) setting a minimum cloud mass of about $10^5\,\mathrm{M}_\odot$ for a galaxy with mass comparable to that in our M33 model. For the standard simulation presented here, the conduction limit thus lies below the resolution limit imposed by the SPH smoothing volume (and slightly above the resolution limit for the simulation with splitting in 32 particles. The number of small clouds is therefore expected to be lowered due to conduction.). At a very high resolution, conduction would provide a natural cut-off scale and allow detailed numerical convergence.

4.2.3 Cooling below 10^4 K?

Although we used a lower cut-off in the cooling function to prevent fragmentation, it is interesting to investigate the fate of the clouds below that temperature. In order to do that, we used a 'standard' cooling function (e.g. Dalgarno & McCray 1972) to derive an estimate for the cooling time-scale of the clouds below 10^4 K. We adopted the parametrization of Gerritsen & Icke (1997) for the temperature range of $\log T < 6.2$

$$\Lambda = 10^{-21} n_{\rm H}^2 \left[10^{-0.1-1.88(5.23-\log T)^4} + 10^{-a-b(4-\log T)^2}\right] \tag{5}$$

in erg cm^{-3} s^{-1}, where a and b depend on the ionization parameter $x = \frac{n_e}{n_{\rm H}}$. The heating term for photoelectric heating of small grains and PAHs (as the largest contributor to the gas heating) is given as $\Gamma = 10^{-24}\,\epsilon G_0\, n_{\rm H}$ in erg cm^{-3} s^{-1}, where ϵ is the heating efficiency and G_0 the incident far-ultraviolet (FUV) field (Bakes & Tielens 1994). The FUV field originates from star formation in the disc; since we are resolving only clouds very close to the disc, we can simply assume that they will be embedded in the same bath of ionizing photons as the rest of the galaxy. With

$$\frac{{\rm d}u}{{\rm d}t} = \frac{\Gamma - \Lambda}{\rho} \tag{6}$$

(Hernquist & Katz 1989), one can give an estimate of the cooling time for such systems neglecting pressure and velocity terms. A typical cloud in our simulation can cool down during its lifetime to several tens of Kelvin for ionization parameters $x \geqslant 0.1$ in less than

1 Myr, for $x \leqslant 0.01$ an equilibrium is reached at several thousand Kelvin. The dynamical time-scale $t_{\rm dyn} = \sqrt{\frac{3\pi}{16G\rho}} \approx 70$ Myr for such a cloud is of the order of its lifetime. Therefore, the clouds could collapse further for $x \geqslant 0.1$ [a value which should be reasonable for the solar neighbourhood (see Cox 1990)]. On the other hand, MB04 find that the extra-galactic ionizing background should prevent the cooling of the clouds below 10^4 K. Self-shielding effects will also be important to decide the ultimate fate of the clouds under the combined action of different heating and cooling mechanisms.

Had we included metals in the simulations, the cooling rate would have been higher. We crudely explored the effect of metals by simply shifting the entire cooling curve up. We found, as expected, that more efficient cooling leads to a larger number of clouds for a given resolution; doubling the energy loss due to cooling (this modified cooling function is somewhere in between primordial gas and gas with solar metalicity) increased the mass and the number in clouds by a factor of the order of 2.7 whereas the mass per cloud and the spatial extent of the clouds remained comparable.

5 CONCLUSIONS

We studied the cooling flow of gas within equilibrium dark plus gaseous haloes. At high resolution, the gas nearly conserves angular momentum and rotates faster as it moves towards the disc. Within 10–20 kpc from the disc, the gas fragments into cold gas clouds pressure confined by the ambient hot halo gas. The clumpy appearance of the gas matches H I observations of outer discs. These cold clouds have similar properties as predicted in analytic models such as that of MB04. However, one difference with MB04 is that the hot gas component is never in approximate hydrostatic equilibrium once it starts cooling and collapsing. This implies, for example, that the disc assembly will occur faster than predicted by a model such as MB04. The mass of galaxies with a given spin should also be different, presumably higher in our case since there is less pressure support against collapse. Unfortunately, a direct comparison in terms of galaxy masses is not possible at this stage since the refined runs that have enough resolution to properly follow the clumpy disc formation have been run only for a very short time-scale. The background gas cools and falls in towards the disc as it loses pressure support. Its radial infall velocity is comparable to that of the cold clouds. This explains why we do not see significant differences in the mass growth of the disc when we compare simulations which yield a very different degree of clumpiness of the accretion flow such as the standard and refined_32 simulations. In our models, the amount of hot gas which is accreted directly to the disc is substantial; however, even after 5 Gyr, there is a residual hot gas halo, such that a large mass fraction of the baryons remains in the halo.

The gas does not accrete on to the disc via a spherically symmetric flow. Rather it flows down in a cylindrical fashion along the angular momentum axis. This is different from that assumed in semi-analytic models for disc formation. The rotational velocity of the gas decreases above the disc plane with a similar velocity gradient as observed in the measurements for NGC 891 by Fraternali et al. (2005). This may be the first evidence for disc formation via radiative cooling of hot gas combined with conservation of angular momentum.

Our simulations show that the thermal instability, and thus the two-phase medium, requires a continuous heating source to be present in order to be maintained, and this is provided here by the gravitational collapse which continuously brings in gas hotter than the gas that has already cooled down. When this heating term is not present, such as in all the cube tests, the instability is rapidly suppressed as the temperature becomes uniform due to the high cooling rate.

We believe that the clouds are stable against the various disruption mechanisms such as conduction and Kelvin–Helmholtz instabilities. The infall velocity of the gas is approximately 10 km s^{-1}. This is much smaller than the pure free-fall velocity towards the disc, $\sim$70 km s^{-1}, owing to the drag exerted by the diffuse hot corona. This velocity can thus be used to measure the ambient hot gas density above the disc plane. This radial infall velocity agrees well with that observed by Fraternali et al. (2002) of approximately 15 km s^{-1} for NGC 2403, a galaxy similar to M33.

In the refined_32 simulation, the sky coverage factor of the clouds is approximately 25 per cent. This is quite similar to the sky coverage factor of high column density HVCs (Richter 2006). The number of cold clouds in our (refined_32) simulation is also similar to those estimated by Putman (2006). However, we caution against overinterpreting these intriguing results. In our model, several physical ingredients that might have an impact on cloud formation, such as gas metalicity, and survival (such as conduction) are still missing, and the initial perturbations are still not determined self-consistently in the mode. It is interesting that cosmological simulations are now beginning to resolve similar structures (Governato et al. 2006; Sommer-Larsen 2006) and that the origin of the perturbations in some of these simulations seems to be dense cold gaseous streams accreted in the process of galaxy formation (Sommer-Larsen 2006). If cold accretion is responsible for the cloud formation, it would have the benefit of being a very general mechanism, although it would occur preferentially in the early stages of their formation for systems as large as the Milky Way today (Kereš et al. 2005).

The growth rate of the cloud masses is approximately linear with time, therefore large initial fluctuations in temperature or density are required. It is likely that the Poisson fluctuations due to discreteness, which are at the 10 per cent level, are coincidentally close to the amplitude of fluctuations required to form $10^6\,{\rm M}_\odot$ clouds within a Gyr. In addition to perturbations of cosmological origin for the clouds to be connected with HVCs, one needs mechanisms that are efficient at any epoch, such as triggering by halo substructure. This includes not only the direct perturbation of sub-haloes moving in the primary halo but also cold gas streams stripped from the baryonic component of the satellites (Mayer et al. 2006). Finally, in order to generate the H I clouds in the extra-planar gas around discs, one also needs local sources of fluctuations such as infalling cold gas or turbulence induced by gravitational perturbations or supernova winds from star formation in the disc. A lot remains to be done to study the role of these different triggering mechanisms which might be simultaneously at play and generate various populations of clouds.

ACKNOWLEDGMENTS

We would like to thank Stelios Kazantzidis for providing a code to generate isolated dark matter haloes and Filippo Fraternali for the rotation curve data for NGC 891. We acknowledge useful and stimulating discussions with Filippo Fraternali, Renzo Sancisi, Frank van den Bosch, Kenneth Sembach, Leo Blitz, Tom Quinn, Fabrizio Brighenti and Fabio Governato. We are grateful to the anonymous referee for his remarks and stimulating comments that considerably improved the paper. The numerical simulations were performed on the zBox (http://krone.physik.unizh.ch/~stadel/zBox) supercomputer at the University of Zürich.

REFERENCES

Abadi M. G., Navarro J. F., Steinmetz M., Eke V. R., 2003, ApJ, 597, 21
Baek C. H., Kang H., Kim J., Ryu D., 2005, ApJ, 630, 689
Bakes E. L. O., Tielens A. G. G. M., 1994, in Cutri R. M., Latter W. B., eds, ASP Conf. Ser. Vol. 58, The First Symposium on the Infrared Cirrus and Diffuse Interstellar Clouds. Astron. Soc. Pac., San Francisco, p. 412
Balsara D. S., 1995, J. Comput. Phys., 121, 357
Barnes J. E., 2002, MNRAS, 333, 481
Benson A. J., Bower R. G., Frenk C. S., White S. D. M., 2000, MNRAS, 314, 557
Blitz L., Spergel D. N., Teuben P. J., Hartmann D., Burton W. B., 1999, ApJ, 514, 818
Bromm V., 2000, PhD thesis, Yale Univ.
Bullock J. S., Dekel A., Kolatt T. S., Kravtsov A. V., Klypin A. A., Porciani C., Primack J. R., 2001, ApJ, 555, 240
Burkert A., Lin D. N. C., 2000, ApJ, 537, 270
Cox D. P., 1990, in Thronson H. A., Shull J.M., eds, ASSL Vol. 161. The Interstellar Medium in Galaxies. Kluwer, Dordrecht, p. 181
Crampin D. J., Hoyle F., 1964, ApJ, 140, 99
Dalgarno A., McCray R. A., 1972, ARA&A, 10, 375
Dekel A., Birnboim Y., 2004, AIP Conf. Proc. vol. 743. The New Cosmology: Conference on Strings and Cosmology, p. 162
Escala A., Larson R. B., Coppi P. S., Mardones D., 2004, ApJ, 607, 765
Fall S. M., Rees M. J., 1985, ApJ, 298, 18
Fraternali F., Oosterloo T., Sancisi R., Swater R., 2005, in Braun R., ed., ASP Conf. Ser. Vol. 331. Extra-Planar Gas. Astron. Soc. Pac., San Francisco, p. 239
Fraternali F., van Moorsel G., Sancisi R., Oosterloo T., 2002, AJ, 123, 3124
Gerritsen J. P. E., Icke V., 1997, A&A, 325, 972
Governato F. et al., 2004, ApJ, 607, 688
Governato F., Willman B., Mayer L., Brooks A., Stinson G., Valenzuela O., Wadsley J., Quinn T., 2006, preprint (astro-ph/0602351)
Heald G. H., Rand R. J., Benjamin R. A., Bershady M. A., 2005, preprint (astro-ph/0508559)
Hernquist L., Katz N., 1989, ApJS, 70, 419
Katz N., Hernquist L., Weinberg D. H., 1992, ApJ, 399, L109
Katz N., Weinberg D. H., Hernquist L., 1996, ApJS, 105, 19
Kaufmann T., Mayer L., Wadsley J., Stadel J., Moore B., 2006, preprint (astro-ph/0601115)
Kazantzidis S., Magorrian J., Moore B., 2004, ApJ, 601, 37
Kereš D., Katz N., Weinberg D. H., Davé R., 2005, MNRAS, 363, 2
Kitsionas S., 2000, PhD thesis Univ. Wales
Maller A. H., Bullock J. S., 2004, MNRAS, 355, 694 (MB04)
Mayer L., Mastropietro C., Wadsley J., Stadel J., Moore B., 2006, MNRAS, 369, 1021
McCarthy I. G., Babul A., Katz N., Balogh M. L., 2003, ApJ, 587, L75
Mo H. J., Miralda-Escude J., 1996, ApJ, 469, 589
Monaghan J. J., 1992, ARA&A, 30, 543
Murray S. D., White S. D. M., Blondin J. M., Lin D. N. C., 1993, ApJ, 407, 588
Navarro J. F., Benz W., 1991, ApJ, 380, 320
Navarro J. F., Frenk C. S., White S. D. M., 1996, ApJ, 462, 563
Navarro J. F., Steinmetz M., 2000, ApJ, 538, 477
Putman M. E., 2006, ApJ, in press (astro-ph/0603650)
Richter P., 2006, preprint (astro-ph/0602343)
Robertson B., Yoshida N., Springel V., Hernquist L., 2004, ApJ, 606, 32
Sembach K. R. et al., 2003, ApJS, 146, 165
Sommer-Larsen J., Götz M., Portinari L., 2003, ApJ, 596, 47
Sommer-Larsen J., 2006, ApJ, 644, L1
Stadel J., 2001, PhD thesis, Univ. Washington
Steinmetz M., White S. D. M., 1997, MNRAS, 288, 545
Wadsley J., Stadel J., Quinn T., 2004, New Astron., 9, 137
White S. D. M., Frenk C. S., 1991, ApJ, 379, 52

This paper has been typeset from a TEX/LATEX file prepared by the author.